Rapid formation of cell aggregates and spheroids induced by a “smart” boronic acid copolymer

*Adérito J. R. Amaral, and George Pasparakis**

UCL School of Pharmacy, University College London, 29-39 Brunswick Square, London WC1N 1AX, UK

ABSTRACT

Cell surface engineering has emerged as a powerful approach to form cell aggregates/spheroids and cell-biomaterial ensembles with significant uses in tissue engineering and cell therapeutics. Herein, we demonstrate that cell membrane remodeling with a thermoresponsive boronic acid copolymer induces the rapid formation of spheroids using either cancer or cardiac cell lines under conventional cell culture conditions at minute concentrations. It is shown that the formation of well-defined spheroids is accelerated by at least 24 hours compared to non-polymer treated controls, and more importantly, the polymer allows for fine control of the aggregation kinetics owing to its stimulus response to temperature and glucose content. Based on its simplicity and effectiveness to promote cellular aggregation, this platform holds promise in three-dimensional tissue/tumor modeling and tissue engineering applications.

KEYWORDS: cell spheroids, 3D cell culture, cell surface engineering, cell therapy, thermoresponsive polymer, PNIPAAm, boronic acid, tissue engineering

1. INTRODUCTION

Over the years, three-dimensional (3D) cell culture has emerged as a useful model that accurately probes spatial aspects of cell-cell interactions and physiological gradients, and preserves cellular viability, function and phenotype that fail to recapitulate in conventional two-dimensional (2D) culture[1-3]. In addition, 3D cell culture systems can establish an *in vivo* mimicking microenvironment that provides deeper insights into cell differentiation, proliferation and migration that allow for a more realistic disease and organ modeling for cell therapeutics and drug screening applications[4-5].

In particular, cell spheroids have found numerous applications in tissue engineering, cell transplantation studies and the development of avascular tumor models[6-8]. Various approaches have been developed to induce cellular aggregation using either "passive" or "active" methods, which comprise stationary culture on non-adherent microstructures[9-11] or thermoresponsive polymeric surfaces[12-14], rotating flasks and bioreactors[15], suspension[16] and hanging-drop culture protocols[17-18]. However, these methods often require days to form robust spheroids or are labor and cost-intensive[19]. Alternative methods comprising microfluidics[20-23], or magnetic[24-26] forces have also been reported that significantly improve the speed and cost of spheroid formation, but in most cases, specialized equipment and culture conditions are required, which are not always available in most biomedical laboratories.

Chemical derivatization of the cell membrane constitutes a powerful approach to selectively induce and control the aggregation of cell populations in a highly controlled manner[27-30]. Cell surface engineering methods have been reported that induce cellular aggregation *via* membrane biotinylation[31-32], covalent crosslinking[33-36], Coulombic/ionic interactions[37-39], or nucleic acid recognition[40-42]. Recently, we reported on new polymers that act as macromolecular crosslinkers of cell populations either by exploiting the covalent derivatization of the cell membrane by suitable succinimide chemistries or by the covalent but reversible membrane modification *via* the formation of boronate esters[43].

In this work, we report on a new copolymer that considerably accelerates the cell aggregation process *via* two distinct mechanisms, namely, the formation of boronate ester crosslinks on the cell membrane and a thermally triggered acceleration of the kinetics of aggregation owing to the hydrophobic interactions above the lower critical solution temperature (LCST) of the polymer. The copolymer is found to induce the rapid formation of cell aggregates (CAs) and well-defined spheroids at significantly lower incubation times compared to non-treated controls under common cell culture conditions; the polymer responds sharply to stimuli such as temperature and glucose, which allows for precise control of the kinetics and the size of the aggregates. More importantly, it is demonstrated that the method is insensitive to the cell line used, which renders the concept generic, implying that the proposed polymer could find applications in a diverse range of research fields, such as the development of micro-tissues, 3D tumoroid and/or organ modeling, and cell therapeutics[44-45].

2. EXPERIMENTAL SECTION

2.1. Materials. All solvents and reagents were purchased from Sigma-Aldrich unless otherwise stated and used as supplied. 3-(acrylamido)phenylboronic acid (APBA) (98%), 2,2′-azobis(2-methylpropionitrile) (AIBN) (98%), diethyl ether (≥99.5%), dimethyl sulfoxide (DMSO) (anhydrous, ≥99.9%), dimethyl sulfoxide-d_6 (DMSO-d_6) (D 99.9%, Cambridge Isotope Laboratories), Dulbecco's modified Eagle's medium (DMEM) (Gibco), Dulbecco's phosphate buffered saline (PBS), D-(+)-glucose, *N*-isopropylacrylamide (NIPAAm) (97%), ethanol (EtOH) (96%, Fisher), fluorescein O-methacrylate (fluorescein-MA) (97%), foetal bovine serum (FBS), LIVE/DEAD® cell-mediated cytotoxicity kit (Life Technologies), penicillin-streptomycin solution, resazurin sodium salt and 0.25% (w/v) trypsin-EDTA solution.

2.2. Polymer synthesis and characterization. *Typical procedure for the synthesis of poly(NIPAAm-co-APBA) (P1).* In a round-bottom flask, NIPAAm (1.12 g, 9.90 mmol) and APBA (19 mg, 0.1 mmol) at molar ratios 99:1 were dissolved in a 1:1 (v/v) DMSO/EtOH mixture (5 mL). AIBN (16 mg, 0.1 mmol) was added to the flask, which was then sealed with a rubber septum before purging with argon for 10 minutes. The reaction mixture was placed in a pre-heated oil bath at 75 ºC for 15 hours to initiate polymerization under magnetic stirring. The polymer was recovered by exposing the reaction to room temperature followed by precipitation in excess diethyl ether and drying under vacuum. The copolymer was isolated as white powder (yield 78%, SEC M_n 35900 Da).

2.3. Cell culture. H9c2(2-1) (rat heart myoblasts) and HepG2 (human hepatocellular carcinoma) cell lines were maintained at 37 ºC, under 5% CO_2 humidified atmosphere, in Dulbecco's modified eagle's medium (DMEM) supplemented with 10% (v/v) heat-inactivated

foetal bovine serum (FBS), penicillin (100 units/mL) and streptomycin (100 μg/mL). Cells were kept subconfluent by allowing recovery every 2-3 days.

2.4. Cell viability assays. The cell viability under the different experimental conditions was assessed in parallel experiments by a resazurin assay as outlined below. Briefly, 48 or 72 hours post-treatment, the cells were incubated with DMEM containing 2% (v/v) resazurin dye. After a 2 hours incubation period at 37 ºC, the absorbance (A) of the medium was measured at 570 nm and 600 nm. The cell viability was calculated as the percentage of the non-treated control cells, according to the formula: $(A_{570}\text{-}A_{600})$ of treated cells × 100 ÷ $(A_{570}\text{-}A_{600})$ of control cells.

Live/Dead assay. Briefly, the cellular aggregates/spheroids were co-stained with $DiOC_{18}$ (2 mM) and propidium iodide (4 mM) for live (green color) and dead (red color) cells, respectively, according to the manufacturer's protocol, and images were acquired by fluorescence microscopy.

2.5. Cellular aggregates formation. The cells were grown to confluence, trypsinized and resuspended in complete culture medium. The copolymer was dissolved in phosphate buffered saline (PBS) solution (pH 7.4, 0.01 M), sterilized and then added into the cells' suspensions at different concentrations (ranging from 25 μg/mL to 500 μg/mL). The polymer-cell suspensions were then transferred to a 48-well plate at a final concentration of $5x10^4$ cells/mL, gently agitated and observed under the optical microscope for various times below (25 ºC) and above (37 ºC) the polymer's LCST.

Spheroids formation. H9c2 cells were incubated with P1 and transferred to ultra-low attachment 24-well plates (Costar® flat bottom) or 96-well plates (Nunc™ Sphera™), and gently agitated. Aggregated cells with different densities ($2x10^3$, $5x10^3$ and $1x10^4$ cells per well) were cultured at 37 ºC in a 5% CO_2 humidified atmosphere. Spheroids morphology was observed by phase-contrast microscopy at regular time points.

2.6. Quantitative analysis of cell aggregation. The cell aggregates' surface area of the main cluster was quantified using ImageJ open source software (National Institute of Health, USA). To evaluate the ratio of cellular aggregation at different time points, the values of the areas were normalized to those of the final aggregated area for 25 μg/mL P1-treated cells (at 90 minutes incubation time), and shown as percentage.

The viability of spheroids was determined by a Live/dead assay as previously described. The spheroids were observed by fluorescence microscopy and the cell viability was quantified with ImageJ and presented as a percentage of the ratio of the number of green pixels to the sum of green and red pixels.

2.7. Statistical analysis. The data are presented as mean ± standard deviation (SD) and analysed using the SPSS® Statistics Software (version 21). Statistical significance of differences was evaluated by one-way ANOVA using Bonferroni or Games-Howell *post hoc* tests. The level of significance was set at probabilities of $^{*}p<0.05$, $^{**}p<0.01$, and $^{***}p<0.001$.

3. RESULTS AND DISCUSSION

3.1. Synthesis and characterization of PNIPAAm-APBA copolymer. The copolymer P1 (Figure 1a) was synthesized by free radical polymerization (FRP) from commercially available monomers, namely, *N*-isopropylacrylamide (NIPAAm) and 3-(acrylamido)phenylboronic acid (APBA)[46]. The final product was isolated in good yield and the chemical composition of the polymer was confirmed by ^{1}H NMR, which showed characteristic aromatic proton peaks in the region 6.9-7.7 ppm, and typical peaks of the isopropyl NIPAAm residues at 0.9 and 3.8 ppm (SI, Figure S1). These peaks were used to determine the ratio of the two co-monomers on the

polymer backbone, which was found to be 98.3:1.7 (NIPAAm:APBA), similar to the initial monomer feed.

The LCST onset of the polymer in PBS and DMEM was determined by UV/Vis spectroscopy and was found to be 32 ºC and 34 ºC, respectively (Figure 1b). It should be noted that the LCST value in PBS (pH 7.4, 0.01 M) is very close to values reported for PNIPAAm homopolymers in water[47], which means that the ionic strength of the PBS used was not sufficient to induce significant salting-out effects[48-49]; the low APBA feed (1.7%) was also not sufficient to lower the LCST onset, despite its hydrophobic character. In addition, given that the ratio of propagation and termination rate constants of acrylamide monomers is considerably higher than that of styrenics[50], implied that the APBA distribution across the polymer chain is not uniform and therefore the overall phase transition of the final product is likely to behave similarly to PNIPAAm homopolymer analogs[51]. On the other hand, the impact of the boronate residues on the LCST onset is apparent in DMEM, which contains glucose. The glucose-boronate esters formed increase the overall solubility of the polymer that shifts the LCST onset to higher temperature[52-53], as observed in Figure 1b. Finally, the phase transition of the polymer in DMEM is complete at 36 ºC, that is, below cell culture conditions, allowing for a good temperature and pH-working window to interact with cells *in vitro*.

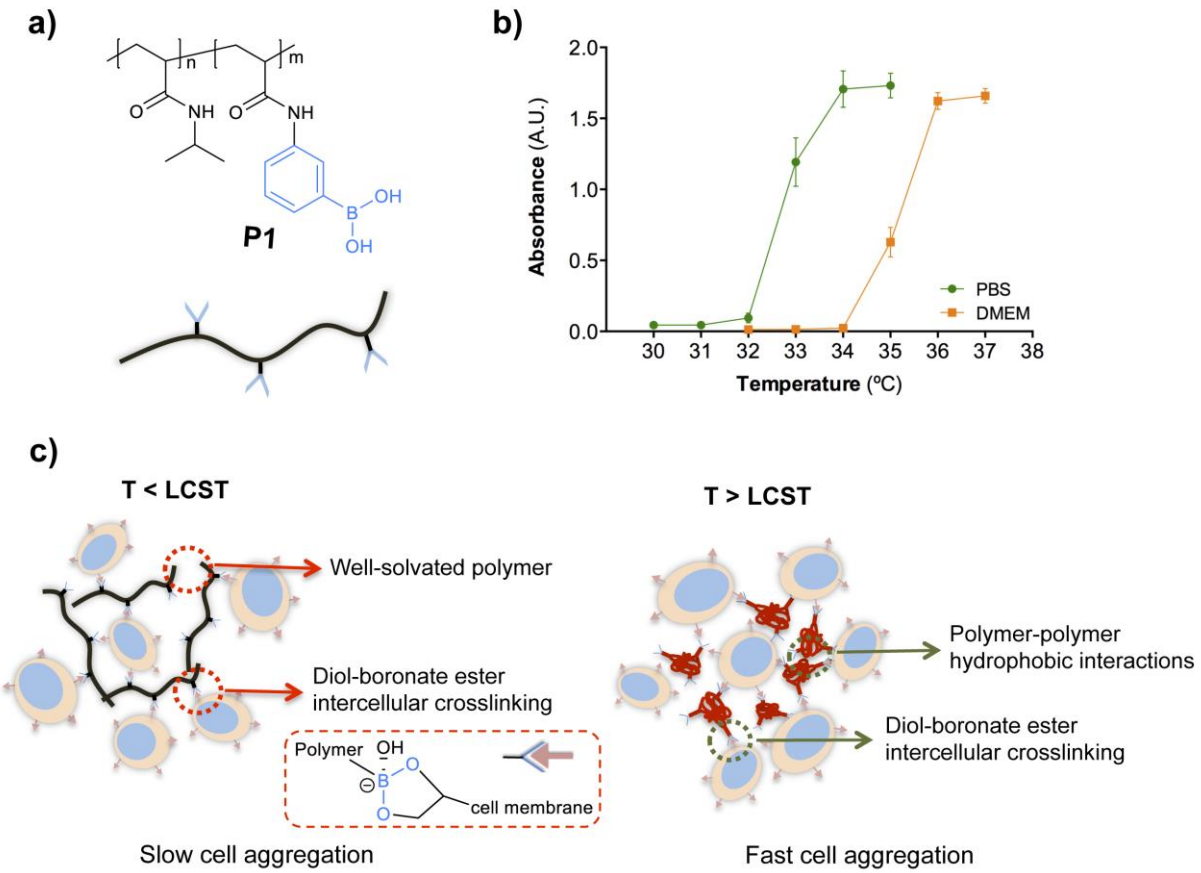

Figure 1. (a) Structure of the thermoresponsive copolymer and (b) phase behavior in PBS (pH 7.4) and DMEM solutions (mean ± SD from triplicates). (c) Schematic diagram of the formation of cell aggregates: macromolecular cell surface modification with P1 induces cell aggregation through intercellular diol-boronate ester crosslinking and thermoresponsive coil-to-globule phase transition.

3.2. Cytotoxicity assessment of copolymer. The cytocompatibility of the copolymer was assessed through the resazurin assay (Figure 2). Cells were incubated with P1 at concentrations ranging from 25 to 1000 µg/mL over a 7-day culture period. After 48 hours, high cell viabilities (around 99%) were observed for all P1 concentrations, while after 72 hours, a minimal decrease was observed with an overall cell viability above 80%. The cytotoxicity assay performed on

H9c2 (cardiomyoblasts) cell line confirmed that the polymer exhibited minimum cytotoxicity, even at concentrations significantly higher than the required to induce cell aggregation.

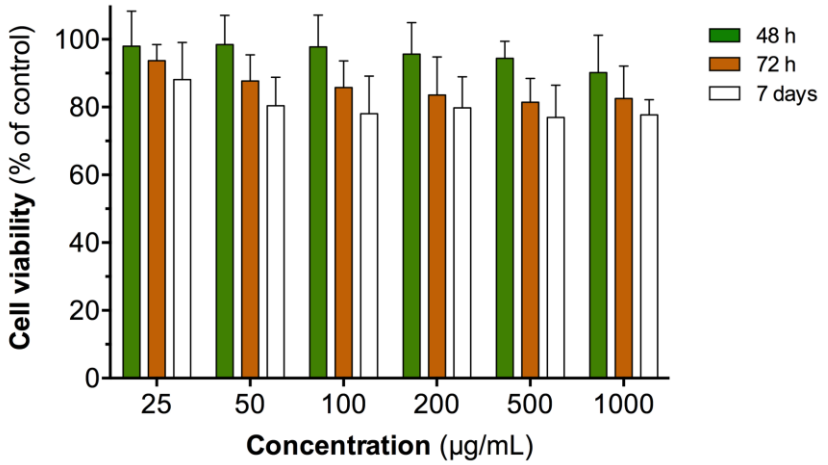

Figure 2. Effect of copolymer concentration on cell viability (H9c2 cell line). The data are expressed as percentage of cell viability with respect to the control corresponding to non-polymer-treated cells (mean ± SD obtained from triplicates).

3.3. Polymer-induced formation of cell aggregates. Cellular aggregation studies were first conducted using H9c2 cells as a model. The formation of CAs was achieved by simple mixing of P1 at low concentrations (25 µg/mL) with cells suspended in complete culture medium. P1 was found to rapidly induce the formation of large CAs at relatively short times, at temperatures above (37 ºC) and below the LCST (25 ºC), as shown in Figure 3a-h. Detailed monitoring of the CAs formation kinetics revealed that P1 could form larger aggregates above the LCST compared to the experiments performed at room temperature. Hence, we concluded that P1 induces aggregation mainly *via* two driving forces: 1) the inter-cellular crosslinking of neighboring cells by the formation of reversible diol-boronate ester bonds with the sialic acids (or other *cis*-diol-rich residues) on cell surface glycoproteins[54-58], and 2) the hydrophobic interaction of the

polymer chains driven by the coil-to-globule phase transition above the LCST[59-63], which further augments the formation of the CAs (Figure 1c). The specificity of the interaction was further confirmed by observing cells without any polymer (Figure 3i, j) or by mixing cells with a PNIPAAm homopolymer (Figure 3k, l), where the absence of CAs was confirmed below and above the LCST. To investigate the attachment of the copolymer on the cell membrane, a fluorescent P1 derivative was synthesized. A characteristic green fluorescent signal was observed at 1 hour incubation time, indicative of the specific interaction of the polymer with the cell membrane. (SI, Figure S2). Finally, in order to probe the role of the diol-boronate ester bond in the formation of CAs, competition experiments with free glucose added in P1-cell suspensions were performed to determine the minimum concentration of free glucose required to completely inhibit the formation of CAs (SI, Figure S3), which was found to be significantly higher (0.1 M) than the existing glucose concentration in the culture medium (0.02 M).

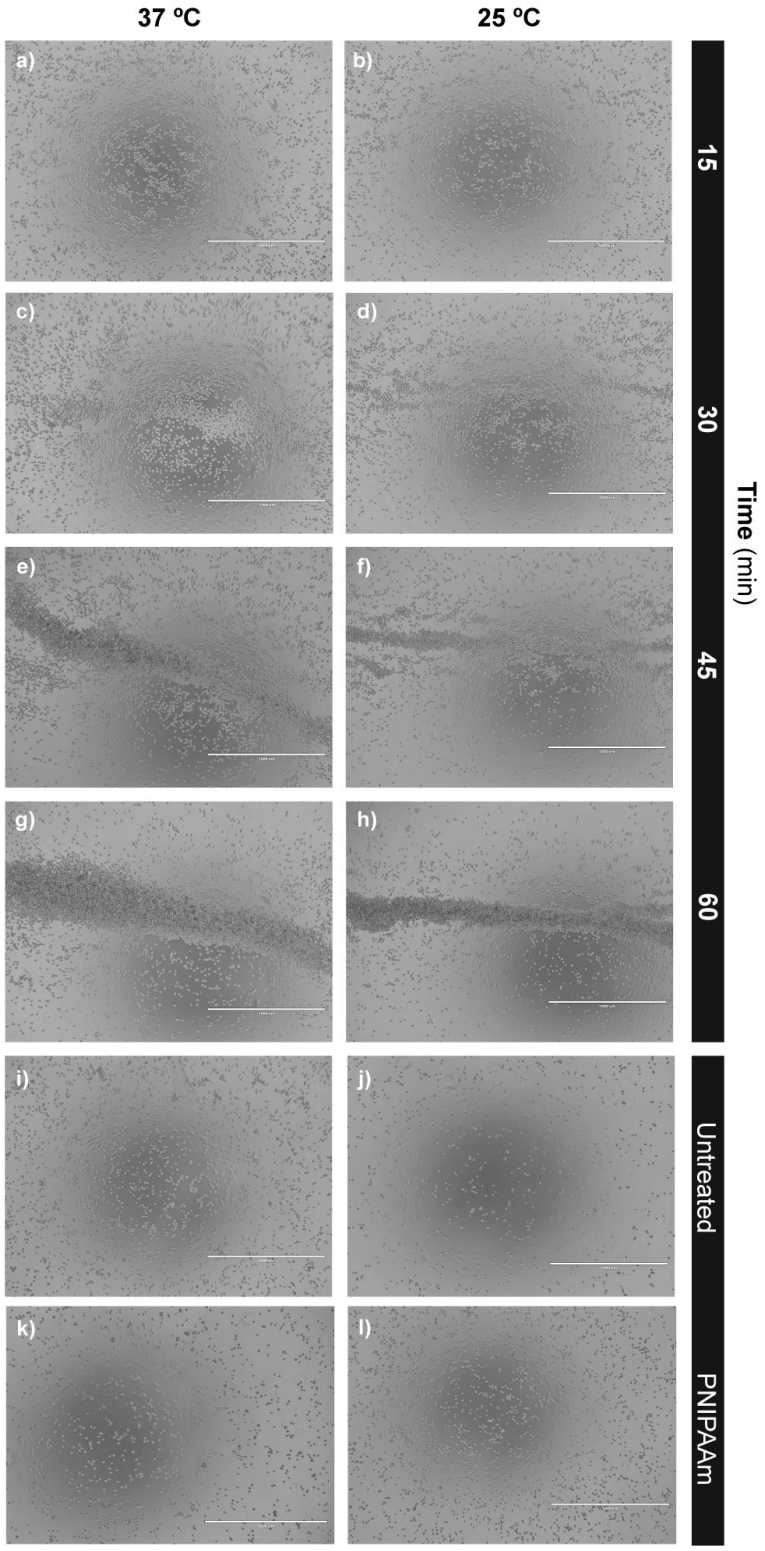

Figure 3. (a-h) Representative phase-contrast microscopy images of H9c2 cell aggregates formation over time at 37 ºC and 25 ºC by addition of 25 μg/mL of P1. (i, j) Control (non-

treated) cells and (k, l) PNIPAAm homopolymer-treated cells after 60 min incubation period (scale bars = 1 mm).

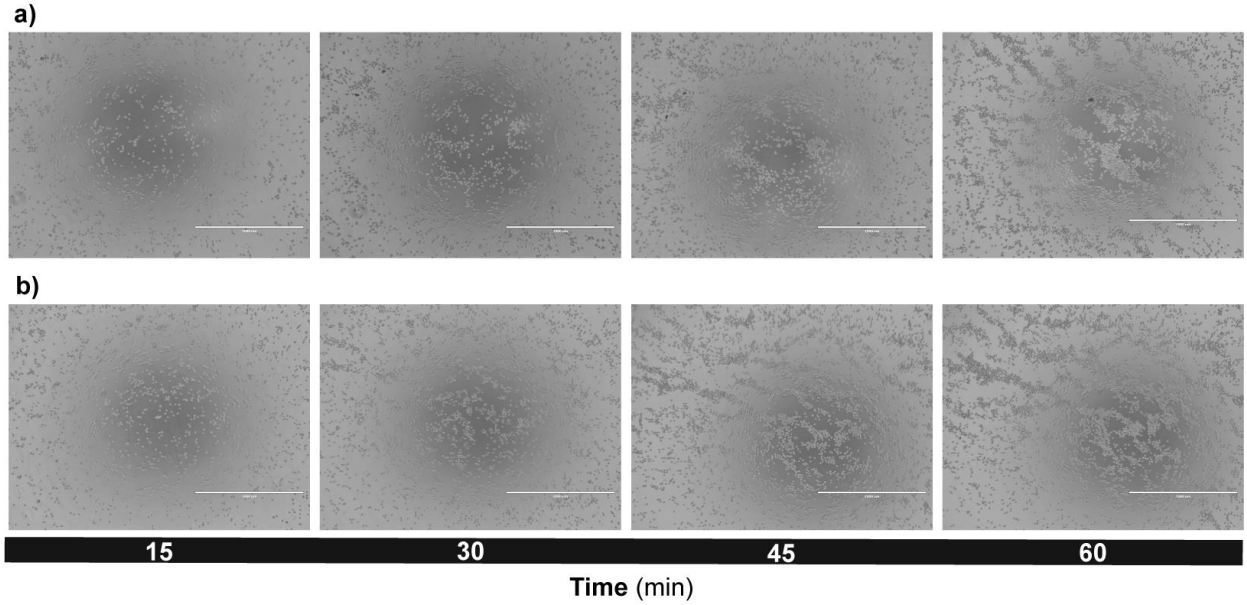

Figure 4. Microscopy images of cell aggregates formation in presence of 200 μg/mL of P1 at (a) 37 ºC and (b) 25 ºC (scale bars = 1 mm).

3.4. Effect of polymer concentration on cellular aggregation. To further elucidate the role of the copolymer concentration on the aggregation mechanism, cells were incubated with P1 at increasing concentrations (25 μg/mL to 500 μg/mL) below and above the LCST. Although P1 could induce extensive CAs formation at 25 and 50 μg/mL as discussed previously, the further increase of P1 concentration (for example at 100 μg/mL or above, as shown in Figure 4), triggered an interesting phenomenon in the aggregation process: the average size of the cell aggregates was significantly reduced, while at polymer concentrations of 500 μg/mL no cell aggregates were observed. We attribute this observation to the steric effect[64] where free non-cell-anchored polymer chains inhibit the interaction of cell bound polymer chains resulting in the

macroscopic prevention of cell aggregate formation. Therefore, we decided to systematically probe the effect of temperature below and above the LCST at different polymer concentrations in more detail (Figure 5).

At P1 concentrations up to 200 μg/mL, an increasing size of CAs over time was observed for both temperatures but at different rates. As expected, the aggregation rate was significantly more pronounced when the temperature was above the polymer's LCST, particularly, at concentrations of P1 below 100 μg/mL. A closer look reveals that after 30 minutes, the average aggregate size almost doubles in comparison with the same conditions below the LCST, while after 60 minutes the CAs formation is completed. At 200 μg/mL of P1, moderate formation of CAs is observed, which does not exceed 45 % of the total area of aggregation (considering as 100% the incubation of cells with P1 at 25 μg/mL) after 90 minutes irrespective of the temperature incubation. Finally, at 500 μg/mL, nearly no CAs are observed after 90 minutes of incubation.

From this set of data, it is proposed that CAs are composed by three phases: a transient organization of discrete small cell clusters forming in the first 15 minutes, followed by a nearly linear growth of the CAs between 15-60 minutes, and a final ripening phase of established aggregate growth taking place after 60 minutes incubation.

To demonstrate the generic nature of the proposed aggregation mechanism, we also performed the experiments on a hepatoma cell line (HepG2). P1 also induced rapid formation of aggregates at similar rates as observed in the case of the H9c2 cell line (SI, Figure S4), which further corroborates our proposed concept that the diol-boronate type of macromolecular cell surface remodeling could indeed serve as a general one-polymer-fits-all approach for mammalian cell lines.

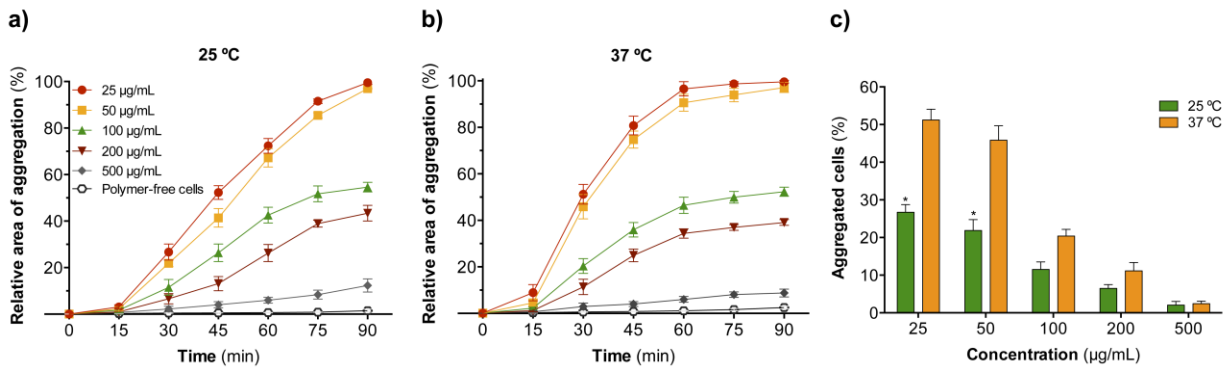

Figure 5. Variation of the degree of aggregation of H9c2 cells with 25 – 500 µg/mL P1 at (a) 37 ºC and (b) 25 ºC at various time points. The cells aggregated rapidly and were tightly packed within 30 min above the LCST. Afterwards, the rate of aggregation gradually decreased, but did not stop until approximately 60 min. (c) Direct comparison of cell aggregation at different concentrations of P1 at 37 ºC *vs.* 25 ºC at 30 min. All values are expressed as mean ± SD of three experiments ($^{*}p<0.05$).

3.5. Cell viability and proliferation of the aggregates in culture. Encouraged by the cell aggregation results, cytotoxicity studies of the CAs formed with P1 at different concentrations were performed using a resazurin assay. Twenty-four hours after aggregation, cell death rates were found to be statistically insignificant, as observed in Figure 6. However, 72 hours post-formation, the death rates significantly increased (*ca.* 30%) for low polymer concentrations as a result of the prominent aggregation process, while low cell death rates (around 10-20%) were observed for high concentrations of P1, where the CAs density and size is lower (Figure 6c). These results underline the fact that low polymer concentrations exert a stronger effect on the aggregation mechanism, which in turn results in higher cell death rates, implying that it is the aggregation process that leads to increased cell death rates and not the polymer itself.

Furthermore, the viability of these CAs was also assessed using a Live/dead assay. Figure 6 also shows that the majority of the cells in the aggregates were viable after a 24 hours incubation period with P1, while at 72 hours, the cell viability decreased. Both assays demonstrated high cell viability 24 hours after CAs formation followed by a steady decrease of the cell viability over time, especially for low concentrations of P1. This trend can be correlated with the average size of the CAs, which increases inversely with P1 concentration and in turn triggers hypoxia conditions at the center of the aggregates, leading to lack of nutrients and oxygen of the innermost cells. This phenomenon is more clearly demonstrated in experiments that involved the formation of cell spheroids with the use of P1 (see below). Although the fluorescence microscopy images of the CAs show an increase of cell death after 72 hours, it is interesting to note that there are more dead cells found with the resazurin assay compared with the live/dead fluorescence assay. We attribute this difference to the fact that non-polymer-treated cells could have proliferated more than those in the CAs, which results in the decrease of the overall cell viability ratio, especially for low concentrations of P1.

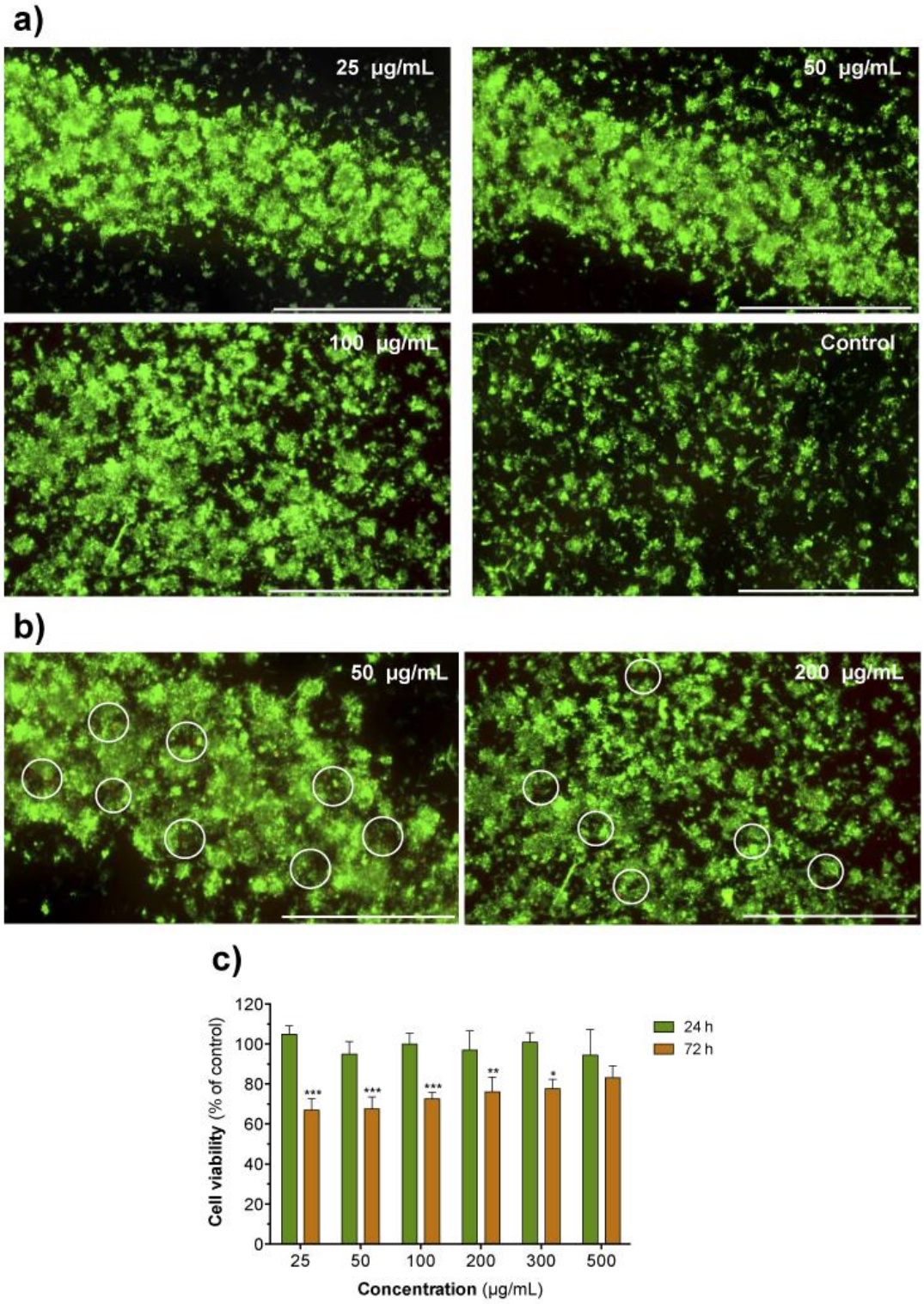

Figure 6. Live/dead fluorescence images of P1-treated cells after (a) 24 h and (b) 72 h. Live cells are shown as green, while dead cells are stained in red (in white circles for optical guidance)

(scale bars = 1 mm). (c) Cell viability studies using resazurin assay at 24 h and 72 h after the formation of the CAs. The data are expressed as percentage of cell viability with respect to the control corresponding to untreated cells (mean ± SD obtained from triplicates). Asterisks ($^{*}p<0.05$, $^{**}p<0.01$, and $^{***}p<0.001$) indicate values that differ significantly from the control.

3.6. Spheroids formation and self-organization. Having established the conditions required to form robust CAs using P1, we sought to test the capability of the copolymer to form scaffold-free tumor spheroid/cardioid models by using non-adherent well plates, which are widely used for the growth of cell aggregates/spheroids.

Figure 7 and Figure 8 illustrate the formation of spheroids comprising H9c2 cells in ultra-low attachment (ULA) flat and round bottom microplates, respectively.

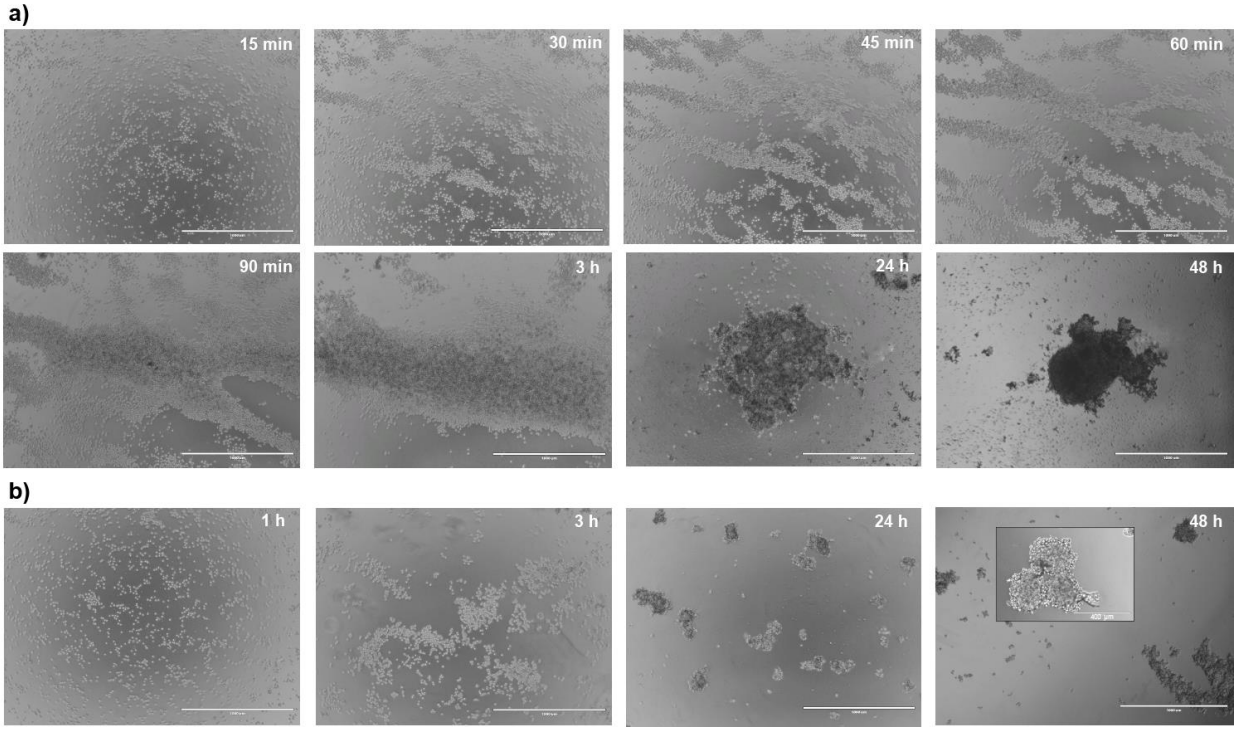

Figure 7. Microscopy images of cell spheroids culture on ULA flat bottom culture plates in time sequence treated with (a) P1 (25 μg/mL) and (b) polymer-free cells (scale bars = 1 mm). The cells were seeded at a concentration of $5x10^4$ cells per well.

In the ULA flat surface, a significant degree of aggregation between cells can be observed even 30 minutes post-seeding. The cells further agglomerate to form a more compact CA after 1 hour, which continues to grow gradually. Subsequently, the aggregate formed a large compact spheroid-like structure with indistinguishable cell-cell boundaries by day 2 (Figure 7a).

The minute addition of polymer into the cells suspension seems to promote the spheroid formation. Microscopy visualization of polymer-free cell cultures show that only small clumps of cells were formed after 24 hours, which contrast with the large and dense aggregates created with P1-treated cells at the same time period. Interestingly, the control samples could not form large and well-defined cell spheroids after 48 hours incubation period (Figure 7b), which clearly signifies the role of P1 in the acceleration of the maturation period of the formation of spheroids under the tested conditions.

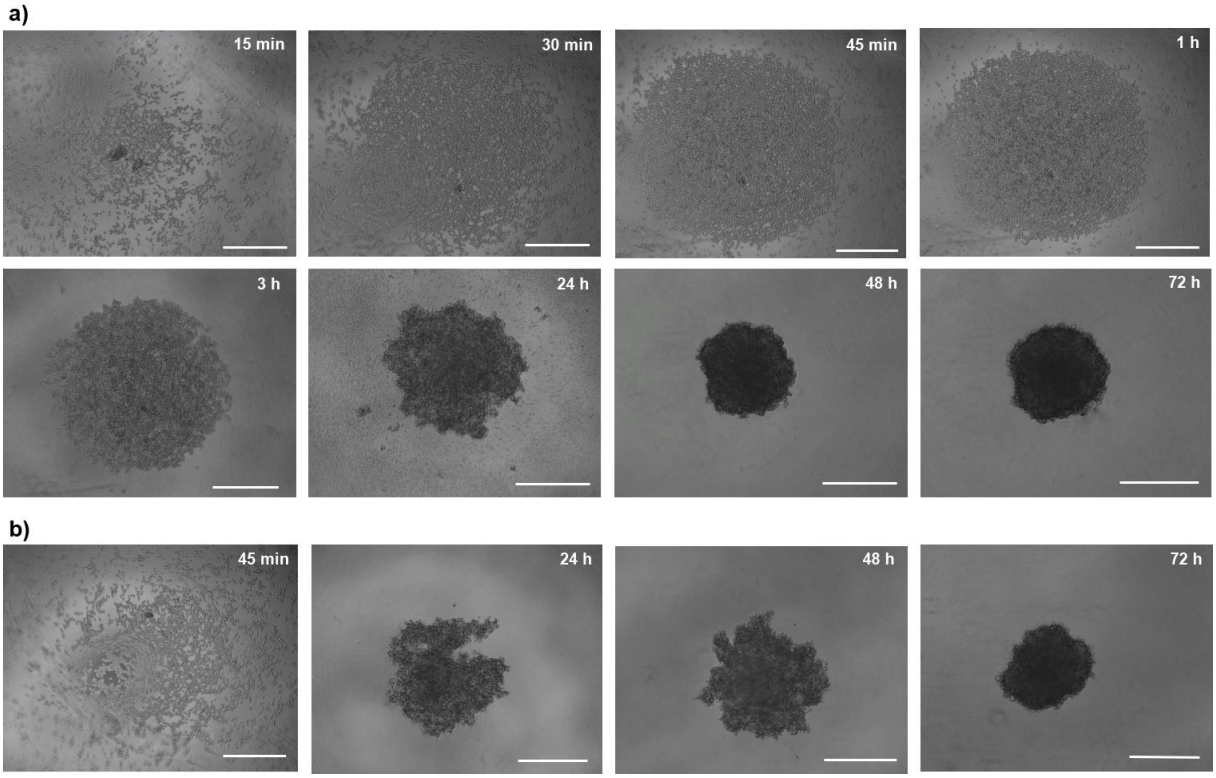

Figure 8. Micrographs of spheroids culture on ULA U-shaped bottom plates treated with (a) P1 (25 μg/mL) and (b) polymer-free cells (scale bars = 500 μm). The aggregates were formed at a cell seeding density of $1x10^4$ cells per well.

To monitor whether P1 influences the kinetics of construction of spheroids in U-shaped ULA surfaces, we incubated the cells with or without P1, and observed them under the microscope over time, as shown in Figure 8.

Strikingly, the most active period of aggregation occurred in the first 60 minutes for the P1-treated cells, where a clear spherical pattern of cells was observed. This rate was significantly higher than that observed for the untreated cells, where it was found that the cells aggregated in a much slower rate and formed less well-defined spheroids 48 hours post-incubation. Again, it is concluded that P1 significantly accelerates the formation of cell spheroids by at least 24 hours in

the round-shaped well plates. Nearly indistinguishable spheroids between polymer treated and non-treated samples are obtained only after 72 hours (Figure 8).

3.7. Quantitative analysis of the cell aggregates/spheroids. Further, we conducted quantitative analysis of the cellular aggregated area in flat and round shaped well plates. It was found that the size of the overall area was independent of P1 concentration (in the range 25-200 μg/mL, Figure 9a), 48 hours post-incubation. More importantly, P1 resulted in a nearly 3-fold increase in the aggregated area compared to the polymer-free control ($^{**}p<0.01$), after 48 hours incubation time (flat bottom plates).

In the case of the cells incubated in U-shaped surface plates, it was found that after 24 hours, the projected area differences between polymer-treated and non-treated cells were not statistically significant and the spheroids were almost identical (Figure 9b). Significant compaction of the cell spheroids was more obvious by day 2, as evidenced by the significant reduction of the diameter. This reduction of the average size after 48 hours is probably attributed to the fact that we capture image areas within the x-y axes of the optical plane of the microscope, which means that if the cells continue to grow in a spheroid-type of geometry (which indeed is evidenced by the characteristic darkening hue of the spheroids under the optical microscope), they should increase their overall volume along the z-axis that is virtually impossible to capture with the optical microscope. Therefore, from this set of experiments, we conclude that gravitational force is probably the main driving mechanism for the spheroid formation in the U-shaped well plates, which undermines the polymer-augmented cell-cell interactions that were observed in the flat ULA surfaces. However, a careful inspection of the microscopy images shows that the polymer formed cell spheroids in the round ULA well plates that exhibit faster

maturation (as evidenced by the darker hue of the spheroids under the optical plane, Figure 8 and Figure 10, at 48 and 72 hours incubation time) and have better defined texture, regardless of the fact that their average sizes at the same time periods are not significantly different from their non-polymer treated counterparts.

Another phenomenological conclusion is that the cells first agglomerate in a large 2D-like aggregate, which at later stages is transformed into a compacted spherical aggregate, implying that there should be an intra-spheroid mechanism that results in the re-organization of the 2D structure to the well-defined 3D spheroid formation.

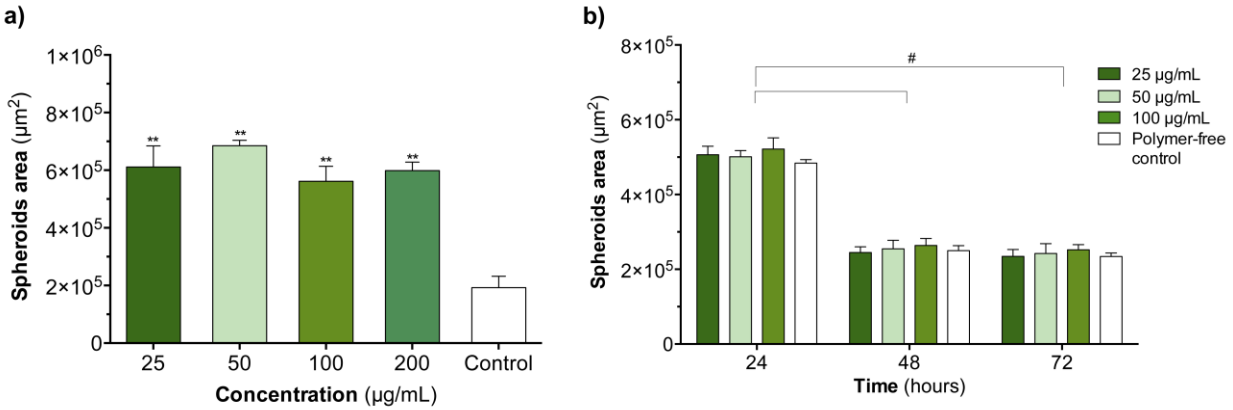

Figure 9. (a) Average spheroids' areas formed with different P1 concentrations in a flat surface plate at 48 h. (b) Average spheroids' surface area as a function of time in U-shaped surfaces. The data are expressed as mean ± SD obtained from three experiments ($^{**}p<0.01$ with control, and $^{\#}p<0.05$ between groups).

3.8. Influence of cell number on spheroid culture. Following the previous results, we explored the relationship between the cell seeding density and the average size of the spheroids

that could be formed (Figure 10). Cell spheroids were formed with P1 at 25 µg/mL using different cell numbers per well ($2x10^3$, $5x10^3$ and $1x10^4$). In all three cell densities tested, well-defined cell spheroids were formed over a period of 48 hours (Figure 10a-c). Interestingly, optical microscopy images revealed an increased compaction of the cells with time, and a well-defined characteristic circular shape with indistinguishable cell boundaries even for the spheroids formed with the lowest number of cells (Figure 10a). As expected, the reduction of the average size of the spheroids was proportional to the decreasing number of cells in each well (Figure 10d), implying that it is possible to design custom-sized spheroids with P1 simply by adjusting the initial cell seeding density.

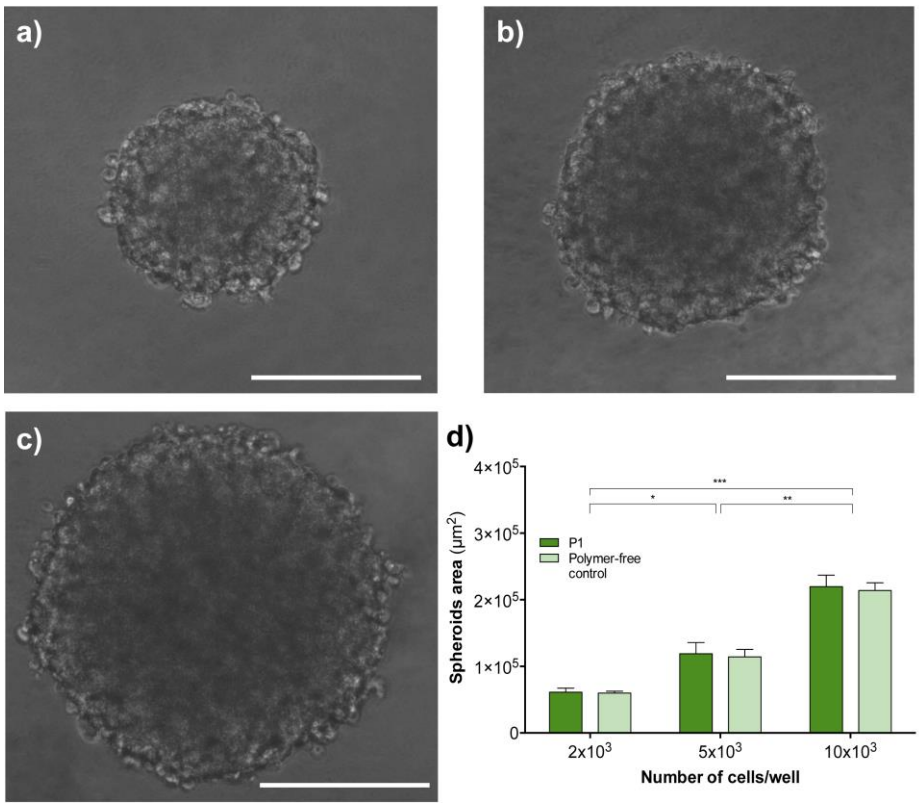

Figure 10. (a-c) Spheroids formed in round bottom microplates with H9c2 cells using $2x10^3$, $5x10^3$ and $1x10^4$ cells per well, respectively; incubation period is 48 h with 25 µg/mL of P1

(scale bars = 200 μm). (d) Average spheroids' area as a function of cell number per well, as determined by optical microscopy. The data are expressed as mean ± SD from three experiments ($^{***}p<0.001$, $^{**}p<0.01$ and $^{*}p<0.05$).

3.9. The fate of 3D cell culture. Next, we examined the viability of the cell spheroids using a Live/dead assay. Figure 11 depicts live/dead fluorescence images of the cell spheroids with different cell seeding densities incubated with P1. The H9c2 spheroids exhibited an overall strong green fluorescent signal corresponding to live cells, although some dead cells (red signal) were also found. Interestingly, most of the cells at the periphery of the spheroids are alive, whereas dead cells are mostly found at the innermost part of the spheroids and are spread evenly within the volume of each spheroid compartment. This color pattern is more noticeable for cell concentrations above $5x10^3$ cells per well. Only 15% of the cells were found dead after 5 days, even for the control polymer-free-formed spheroids, when cell number is *ca.* $2x10^3$. However, *ca.* 40% dead cells were found in spheroids with $1x10^4$ cells per well. These agglomerates with diameters, typically, above 200 μm, develop chemical gradients where the innermost cells become quiescent and eventually die *via* apoptosis or necrosis[65-66], while cells located at the periphery are actively dividing, as is evidenced by the homogenous green layer formed around the spheroids. It was also observed that cellular viability was independent of P1 concentration (SI, Figure S5). It is therefore concluded that there is a strong inverse correlation of the cell viability with the average size of the spheroids, and in order to eliminate extensive cell death within the spheroids, the latter should be preferably designed with relatively low cell seeding densities (i.e., below $5x10^3$ cells per well).

Therefore, our proposed copolymer could find useful applications in the construction of cell spheroids suitable for cell therapeutics, or the modeling of cancer tumoroids and hypoxia patterns[67].

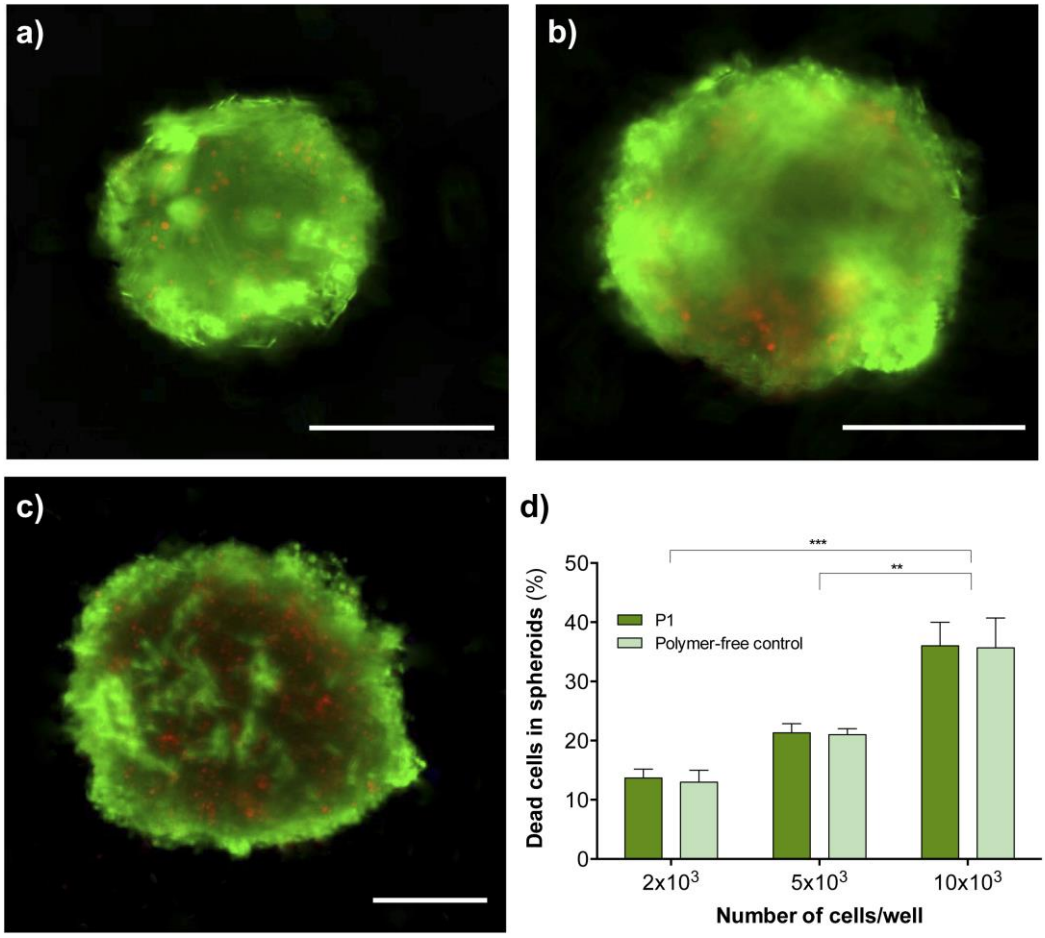

Figure 11. (a-c) Fluorescence microscopy images of the live/dead assay of cell spheroids after 5 days incubation with P1 at 25 μg/mL using $2x10^3$, $5x10^3$ and $1x10^4$ cells per well, respectively (scale bars = 200 μm). (d) Quantification of cell death in the spheroids. The data are expressed as mean ± SD of at least three selected images for each condition ($^{**}p<0.01$ and $^{*}p<0.05$).

In a wider context, the construction of 3D cell culture models for biomedical applications poses several technical challenges depending on the targeted application, which has led to the development of various 3D culture methods. For example, the formation of cell spheroids is usually conducted either by scaffold-based (including hydrogels, patterned constructs, microfluidic devices, *etc.*) or scaffold-free (*e.g.* hanging drop method, rotating bioreactors, among others) methods that have their own merits in terms of applicability, scalability and cost. We believe that our proposed method can be integrated with many of the aforementioned methods as it has certain advantages in that 1) it comprises a non-toxic synthetic polymer that exerts strong cell-cell aggregation motifs at micromolar concentrations, 2) it accelerates significantly the complete formation of cell aggregates/spheroids (for example, as it was demonstrated in ULA surfaces where the formation time was faster by at least 24 hours), 3) it is perfectly compatible with widely used cell culture kits and sera, 4) it is generic regardless of the cell line as virtually most cell lines have glycosylated residues on their cell membrane, which are all potential chemical anchors of the boronate-rich polymer, and 5) it exerts robust aggregate kinetics owing to the covalent nature of the boronate bonds, albeit is highly controllable and reversible by the addition of free glucose or the control of the polymer's LCST onset.

4. CONCLUSIONS

In conclusion, we demonstrated a new thermoresponsive copolymer that induces rapid cell aggregation in complete medium exerted by specific polymer-cell surface interactions. The proposed copolymer can be easily integrated with existing cell culture protocols and significantly accelerates the formation of cell aggregates/spheroids at minute concentrations, under certain conditions. We anticipate that such macromolecular cell surface remodeling approaches will fuel

the field of chemically promoted 3D cellular constructs that could further boost the development of cell culture protocols and methods for tissue engineering, cell therapies, and ex/*in vivo* modeling studies.

ASSOCIATED CONTENT

Supporting Information

Additional experimental details of polymer characterization, cell culture experiments and microscopy images.

AUTHOR INFORMATION

Corresponding Author

*E-mail: g.pasparakis@ucl.ac.uk

Author Contributions

All authors have given approval to the final version of the manuscript.

Notes

The authors declare no competing financial interest.

ACKNOWLEDGMENTS

This work was supported by the Leverhulme Trust (ECF-2013-472) and the UCL Excellence Fellowship program. Dr Gareth Williams (UCL School of Pharmacy) is acknowledged for kindly providing the H9c2 cell line.

REFERENCES

1. Cukierman, E.; Pankov, R.; Stevens, D. R.; Yamada, K. M. Taking Cell-Matrix Adhesions to the Third Dimension. *Science* **2001,** *294*, 1708-1712.

2. Griffith, L. G.; Swartz, M. A. Capturing Complex 3D Tissue Physiology in vitro. *Nat. Rev. Mol. Cell Biol.* **2006,** *7*, 211-224.

3. Tibbitt, M. W.; Anseth, K. S. Hydrogels as Extracellular Matrix Mimics for 3D Cell Culture. *Biotechnol. Bioeng.* **2009,** *103*, 655-663.

4. Mueller-Klieser, W. Three-dimensional Cell Cultures: From Molecular Mechanisms to Clinical Applications. *Am. J. Physiol.: Cell Physiol.* **1997,** *273*, C1109-C1123.

5. Pampaloni, F.; Reynaud, E. G.; Stelzer, E. H. K. The Third Dimension Bridges the Gap Between Cell Culture and Live Tissue. *Nat. Rev. Mol. Cell Biol.* **2007,** *8*, 839-845.

6. Cox, M. C.; Reese, L. M.; Bickford, L. R.; Verbridge, S. S. Toward the Broad Adoption of 3D Tumor Models in the Cancer Drug Pipeline. *ACS Biomater. Sci. Eng.* **2015,** *1*, 877-894.

7. Fitzgerald, K. A.; Malhotra, M.; Curtin, C. M.; O' Brien, F. J.; O' Driscoll, C. M. Life in 3D is Never Flat: 3D Models to Optimise Drug Delivery. *J. Controlled Release* **2015,** *215*, 39-54.

8. Zuppinger, C. 3D Culture for Cardiac Cells. *Biochim. Biophys. Acta, Mol. Cell Res.* **2016,** *1863*, 1873-1881.

9. Liu, T.; Chien, C.-C.; Parkinson, L.; Thierry, B. Advanced Micromachining of Concave Microwells for Long Term On-Chip Culture of Multicellular Tumor Spheroids. *ACS Appl. Mater. Interfaces* **2014,** *6*, 8090-8097.

10. Liu, T.; Yang, C.-T.; Dieguez, L.; Denman, J. A.; Thierry, B. Robust and Flexible Fabrication of Chemical Micropatterns for Tumor Spheroid Preparation. *ACS Appl. Mater. Interfaces* **2014,** *6*, 10162-10171.

11. Fukuda, J.; Sakai, Y.; Nakazawa, K. Novel Hepatocyte Culture System Developed Using Microfabrication and Collagen/Polyethylene Glycol Microcontact Printing. *Biomaterials* **2006,** *27*, 1061-1070.

12. Kikuchi, A.; Okano, T. Nanostructured Designs of Biomedical Materials: Applications of Cell Sheet Engineering to Functional Regenerative Tissues and Organs. *J. Controlled Release* **2005,** *101*, 69-84.

13. Shimizu, T.; Yamato, M.; Isoi, Y.; Akutsu, T.; Setomaru, T.; Abe, K.; Kikuchi, A.; Umezu, M.; Okano, T. Fabrication of Pulsatile Cardiac Tissue Grafts Using a Novel 3-Dimensional Cell Sheet Manipulation Technique and Temperature-Responsive Cell Culture Surfaces. *Circ. Res.* **2002,** *90*, e40-e48.

14. Yamazaki, M.; Tsuchida, M.; Kobayashi, K.-y.; Takezawa, T.; Mori, Y. A Novel Method to Prepare Size-Regulated Spheroids Composed of Human Dermal Fibroblasts. *Biotechnol. Bioeng.* **1994,** *44*, 38-44.

15. Wu, F. J.; Friend, J. R.; Hsiao, C. C.; Zilliox, M. J.; Ko, W.-J.; Cerra, F. B.; Hu, W.-S. Efficient Assembly of Rat Hepatocyte Spheroids for Tissue Engineering Applications. *Biotechnol. Bioeng.* **1996,** *50*, 404-415.

16. Lei, J.; McLane, L. T.; Curtis, J. E.; Temenoff, J. S. Characterization of a Multilayer Heparin Coating for Biomolecule Presentation to Human Mesenchymal Stem Cell Spheroids. *Biomater. Sci.* **2014,** *2*, 666-673.

17. Kelm, J. M.; Timmins, N. E.; Brown, C. J.; Fussenegger, M.; Nielsen, L. K. Method for Generation of Homogeneous Multicellular Tumor Spheroids Applicable to a Wide Variety of Cell Types. *Biotechnol. Bioeng.* **2003,** *83*, 173-180.

18. Lin, B.; Miao, Y.; Wang, J.; Fan, Z.; Du, L.; Su, Y.; Liu, B.; Hu, Z.; Xing, M. Surface Tension Guided Hanging-Drop: Producing Controllable 3D Spheroid of High-Passaged Human Dermal Papilla Cells and Forming Inductive Microtissues for Hair-Follicle Regeneration. *ACS Appl. Mater. Interfaces* **2016,** *8*, 5906-5916.

19. Mueller-Klieser, W. Tumor Biology and Experimental Therapeutics. *Critical Reviews in Oncology / Hematology* **2000,** *36*, 123-139.

20. Anene-Nzelu, C. G.; Peh, K. Y.; Fraiszudeen, A.; Kuan, Y. H.; Ng, S. H.; Toh, Y. C.; Leo, H. L.; Yu, H. Scalable Alignment of Three-Dimensional Cellular Constructs in a Microfluidic Chip. *Lab Chip* **2013,** *13*, 4124-4133.

21. Wang, J.; Cheng, Y.; Yu, Y.; Fu, F.; Chen, Z.; Zhao, Y.; Gu, Z. Microfluidic Generation of Porous Microcarriers for Three-Dimensional Cell Culture. *ACS Appl. Mater. Interfaces* **2015,** *7*, 27035-27039.

22. O'Brien, P. J.; Luo, W.; Rogozhnikov, D.; Chen, J.; Yousaf, M. N. Spheroid and Tissue Assembly via Click Chemistry in Microfluidic Flow. *Bioconjugate Chem.* **2015,** *26*, 1939-1949.

23. Oliveira, M. B.; Neto, A. I.; Correia, C. R.; Rial-Hermida, M. I.; Alvarez-Lorenzo, C.; Mano, J. F. Superhydrophobic Chips for Cell Spheroids High-Throughput Generation and Drug Screening. *ACS Appl. Mater. Interfaces* **2014,** *6*, 9488-9495.

24. Okochi, M.; Takano, S.; Isaji, Y.; Senga, T.; Hamaguchi, M.; Honda, H. Three-Dimensional Cell Culture Array Using Magnetic Force-Based Cell Patterning for Analysis of Invasive Capacity of BALB/3T3/v-src. *Lab Chip* **2009,** *9*, 3378-3384.

25. Hu, K.; Zhou, N.; Li, Y.; Ma, S.; Guo, Z.; Cao, M.; Zhang, Q.; Sun, J.; Zhang, T.; Gu, N. Sliced Magnetic Polyacrylamide Hydrogel with Cell-Adhesive Microarray Interface: A Novel Multicellular Spheroid Culturing Platform. *ACS Appl. Mater. Interfaces* **2016**, *8*, 15113-15119.

26. Ho, V. H. B.; Müller, K. H.; Barcza, A.; Chen, R.; Slater, N. K. H. Generation and Manipulation of Magnetic Multicellular Spheroids. *Biomaterials* **2010,** *31*, 3095-3102.

27. Prescher, J. A.; Dube, D. H.; Bertozzi, C. R. Chemical Remodelling of Cell Surfaces in Living Animals. *Nature* **2004,** *430*, 873-877.

28. Stephan, M. T.; Moon, J. J.; Um, S. H.; Bershteyn, A.; Irvine, D. J. Therapeutic Cell Engineering with Surface-Conjugated Synthetic Nanoparticles. *Nat Med* **2010,** *16*, 1035-1041.

29. Stevens, M. M.; George, J. H. Exploring and Engineering the Cell Surface Interface. *Science* **2005,** *310*, 1135-1138.

30. Kellam, B.; De Bank, P. A.; Shakesheff, K. M. Chemical Modification of Mammalian Cell Surfaces. *Chem. Soc. Rev.* **2003,** *32*, 327-337.

31. Kojima, N.; Takeuchi, S.; Sakai, Y. Establishment of Self-Organization System in Rapidly Formed Multicellular Heterospheroids. *Biomaterials* **2011,** *32*, 6059-6067.

32. Meier, W. Reversible Cell Aggregation Induced by Specific Ligand−Receptor Coupling. *Langmuir* **2000,** *16*, 1457-1459.

33. Stabler, C. L.; Sun, X.-L.; Cui, W.; Wilson, J. T.; Haller, C. A.; Chaikof, E. L. Surface Re-engineering of Pancreatic Islets with Recombinant azido-Thrombomodulin. *Bioconjugate Chem.* **2007,** *18*, 1713-1715.

34. Iwasaki, Y.; Sakiyama, M.; Fujii, S.; Yusa, S.-i. Surface Modification of Mammalian Cells With Stimuli-Responsive Polymers. *Chem. Commun. (Cambridge, U. K.)* **2013,** *49*, 7824-7826.

35. Mo, X.; Li, Q.; Yi Lui, L. W.; Zheng, B.; Kang, C. H.; Nugraha, B.; Yue, Z.; Jia, R. R.; Fu, H. X.; Choudhury, D.; Arooz, T.; Yan, J.; Lim, C. T.; Shen, S.; Hong Tan, C.; Yu, H. Rapid Construction of Mechanically- Confined Multi- Cellular Structures using Dendrimeric Intercellular Linker. *Biomaterials* **2010,** *31*, 7455-7467.

36. Dutta, D.; Pulsipher, A.; Luo, W.; Yousaf, M. N. Synthetic Chemoselective Rewiring of Cell Surfaces: Generation of Three-Dimensional Tissue Structures. *J. Am. Chem. Soc.* **2011,** *133*, 8704-8713.

37. Ciupa, A.; De Bank, P. A.; Caggiano, L. Multicellular Aggregation of Maltol-Modified Cells Triggered by Fe3+ ions. *Chem. Commun. (Cambridge, U. K.)* **2013,** *49*, 10148-10150.

38. Wilson, J. T.; Cui, W.; Kozlovskaya, V.; Kharlampieva, E.; Pan, D.; Qu, Z.; Krishnamurthy, V. R.; Mets, J.; Kumar, V.; Wen, J.; Song, Y.; Tsukruk, V. V.; Chaikof, E. L. Cell Surface Engineering with Polyelectrolyte Multilayer Thin Films. *J. Am. Chem. Soc.* **2011,** *133*, 7054-7064.

39. Ong, S.-M.; He, L.; Thuy Linh, N. T.; Tee, Y.-H.; Arooz, T.; Tang, G.; Tan, C.-H.; Yu, H. Transient Inter-Cellular Polymeric Linker. *Biomaterials* **2007,** *28*, 3656-3667.

40. Chandra, R. A.; Douglas, E. S.; Mathies, R. A.; Bertozzi, C. R.; Francis, M. B. Programmable Cell Adhesion Encoded by DNA Hybridization. *Angew. Chem. Int. Ed.* **2006,** *45*, 896-901.

41. Hsiao, S. C.; Shum, B. J.; Onoe, H.; Douglas, E. S.; Gartner, Z. J.; Mathies, R. A.; Bertozzi, C. R.; Francis, M. B. Direct Cell Surface Modification with DNA for the Capture of Primary Cells and the Investigation of Myotube Formation on Defined Patterns. *Langmuir* **2009,** *25*, 6985-6991.

42. Gartner, Z. J.; Bertozzi, C. R. Programmed Assembly of 3-Dimensional Microtissues with Defined Cellular Connectivity. *Proc. Natl. Acad. Sci. U. S. A.* **2009,** *106*, 4606-4610.

43. Amaral, A. J. R.; Pasparakis, G. Macromolecular Cell Surface Engineering for Accelerated and Reversible Cellular Aggregation. *Chem. Commun. (Cambridge, U. K.)* **2015,** *51*, 17556-17559.

44. Brooks, W. L. A.; Sumerlin, B. S. Synthesis and Applications of Boronic Acid-Containing Polymers: From Materials to Medicine. *Chem. Rev. (Washington, DC, U. S.)* **2016,** *116*, 1375-1397.

45. Stuart, M. A. C.; Huck, W. T. S.; Genzer, J.; Muller, M.; Ober, C.; Stamm, M.; Sukhorukov, G. B.; Szleifer, I.; Tsukruk, V. V.; Urban, M.; Winnik, F.; Zauscher, S.; Luzinov, I.; Minko, S. Emerging Applications of Stimuli-Responsive Polymer Materials. *Nat. Mater.* **2010,** *9*, 101-113.

46. Pasparakis, G.; Vamvakaki, M.; Krasnogor, N.; Alexander, C. Diol-Boronic Acid Complexes Integrated by Responsive Polymers-A Route to Chemical Sensing and Logic Operations. *Soft Matter* **2009,** *5*, 3839-3841.

47. Kubota, K.; Fujishige, S.; Ando, I. Solution Properties of Poly(N-isopropylacrylamide) in Water. *Polym. J. (Tokyo, Jpn.)* **1990,** *22*, 15-20.

48. Zhang, Y.; Furyk, S.; Bergbreiter, D. E.; Cremer, P. S. Specific Ion Effects on the Water Solubility of Macromolecules: PNIPAM and the Hofmeister Series. *J. Am. Chem. Soc.* **2005,** *127*, 14505-14510.

49. Zhang, Y.; Furyk, S.; Sagle, L. B.; Cho, Y.; Bergbreiter, D. E.; Cremer, P. S. Effects of Hofmeister Anions on the LCST of PNIPAM as a Function of Molecular Weight. *J. Phys. Chem. C* **2007,** *111*, 8916-8924.

50. North, A. M.; Scallan, A. M. The Free Radical Polymerization of N,N-Dimethylacrylamide. *Polymer* **1964,** *5*, 447-455.

51. Aoki, T.; Nagao, Y.; Sanui, K.; Ogata, N.; Kikuchi, A.; Sakurai, Y.; Kataoka, K.; Okano, T. Glucose-Sensitive Lower Critical Solution Temperature Changes of Copolymers Composed of N-Isopropylacrylamide and Phenylboronic Acid Moieties. *Polym. J. (Tokyo, Jpn.)* **1996,** *28*, 371-374.

52. Matsumoto, A.; Ikeda, S.; Harada, A.; Kataoka, K. Glucose-Responsive Polymer Bearing a Novel Phenylborate Derivative as a Glucose-Sensing Moiety Operating at Physiological pH Conditions. *Biomacromolecules* **2003,** *4*, 1410-1416.

53. Kataoka, K.; Miyazaki, H.; Okano, T.; Sakurai, Y. Sensitive Glucose-Induced Change of the Lower Critical Solution Temperature of Poly[N,N-(dimethylacrylamide)-co-3-(acrylamido)-phenylboronic acid] in Physiological Saline. *Macromolecules* **1994,** *27*, 1061-1062.

54. Xu, X.-D.; Cheng, H.; Chen, W.-H.; Cheng, S.-X.; Zhuo, R.-X.; Zhang, X.-Z. In Situ Recognition of Cell-Surface Glycans and Targeted Imaging of Cancer Cells. *Sci. Rep.* **2013,** *3*, 2679.

55. Matsumoto, A.; Sato, N.; Kataoka, K.; Miyahara, Y. Noninvasive Sialic Acid Detection at Cell Membrane by Using Phenylboronic Acid Modified Self-Assembled Monolayer Gold Electrode. *J. Am. Chem. Soc.* **2009,** *131*, 12022-12023.

56. Wang, S.; Yin, D.; Wang, W.; Shen, X.; Zhu, J.-J.; Chen, H.-Y.; Liu, Z. Targeting and Imaging of Cancer Cells via Monosaccharide-Imprinted Fluorescent Nanoparticles. *Sci. Rep.* **2016,** *6*, 22757.

57. Liu, H.; Li, Y.; Sun, K.; Fan, J.; Zhang, P.; Meng, J.; Wang, S.; Jiang, L. Dual-Responsive Surfaces Modified with Phenylboronic Acid-Containing Polymer Brush To Reversibly Capture and Release Cancer Cells. *J. Am. Chem. Soc.* **2013,** *135*, 7603-7609.

58. Saxon, E.; Bertozzi, C. R. Cell Surface Engineering by a Modified Staudinger Reaction. *Science* **2000,** *287*, 2007-2010.

59. Roy, D.; Cambre, J. N.; Sumerlin, B. S. Triply-Responsive Boronic Acid Block Copolymers: Solution Self-Assembly Induced by Changes in Temperature, pH, or Sugar Concentration. *Chem. Commun. (Cambridge, U. K.)* **2009**, 2106-2108.

60. Cooperstein, M. A.; Canavan, H. E. Biological Cell Detachment from Poly(N-isopropyl acrylamide) and Its Applications. *Langmuir* **2010,** *26*, 7695-7707.

61. Pasparakis, G.; Vamvakaki, M. Multiresponsive Polymers: Nano-Sized Assemblies, Stimuli-Sensitive Gels and Smart Surfaces. *Polym. Chem.* **2011,** *2*, 1234-1248.

62. Schild, H. G. Poly(N-isopropylacrylamide): Experiment, Theory and Application. *Prog. Polym. Sci.* **1992,** *17*, 163-249.

63. Kong, B.; Choi, J. S.; Jeon, S.; Choi, I. S. The Control of Cell Adhesion and Detachment on Thin Films of Thermoresponsive Poly[(N-isopropylacrylamide)-r-((3-(methacryloylamino)propyl)-dimethyl(3-sulfopropyl)ammonium hydroxide)]. *Biomaterials* **2009,** *30*, 5514-5522.

64. Klein, J.; Luckham, P. F. Long-Range Attractive Forces Between Two Mica Surfaces in an Aqueous Polymer Solution. *Nature* **1984,** *308*, 836-837.

65. Hirschhaeuser, F.; Menne, H.; Dittfeld, C.; West, J.; Mueller-Klieser, W.; Kunz-Schughart, L. A. Multicellular Tumor Spheroids: An Underestimated Tool is Catching Up Again. *J. Biotechnol.* **2010,** *148*, 3-15.

66. Mehta, G.; Hsiao, A. Y.; Ingram, M.; Luker, G. D.; Takayama, S. Opportunities and Challenges for Use of Tumor Spheroids as Models to Test Drug Delivery and Efficacy. *J. Controlled Release* **2012,** *164*, 192-204.

67. Tay, C. Y.; Muthu, M. S.; Chia, S. L.; Nguyen, K. T.; Feng, S.-S.; Leong, D. T. Reality Check for Nanomaterial-Mediated Therapy with 3D Biomimetic Culture Systems. *Adv. Funct. Mater.* **2016**, *26*, 4046-4065.

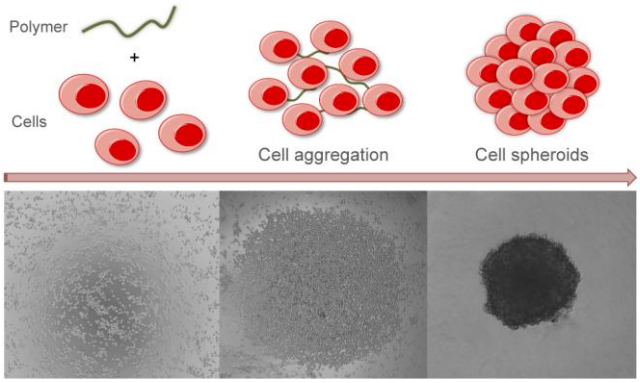

For Table of Contents Only